

High-Efficiency Energy Conversion in a Molecular Triad Connected to Conducting Leads

Anatoly Yu. Smirnov,^{*,†,‡} Lev G. Mourokh,[§] Pulak K. Ghosh,[†] and Franco Nori^{*,†,‡}

Advanced Science Institute, The Institute of Physical and Chemical Research (RIKEN), Wako-shi, Saitama, 351-0198, Japan, Physics Department, Center for Theoretical Physics, The University of Michigan, Ann Arbor, Michigan 48109-1040, and Department of Physics, Queens College, The City University of New York, Flushing, New York 11367

Received: July 20, 2009; Revised Manuscript Received: October 26, 2009

We theoretically examine the light-to-electricity energy conversion in a molecular triad coupled to conducting leads. This coupling allows us to drive a current through the system. We derive the equations of motion for the electron density operators and determine the dependence of the current, quantum yield, and thermodynamic efficiency on temperature, the electrochemical potentials of the leads, as well as on the light intensity and frequency of the external electromagnetic field. For the molecular triad consisting of ferrocene, porphyrin, and fullerene molecules, we find that, in the case of relatively strong coupling to the leads, the power-conversion efficiency can exceed 40% and the quantum yield can be more than 90%, instead of the 25% quantum yield observed in experiments. Thus, this system is highly attractive for solar cell applications. The large predicted increase in the efficiency of this system is due to the stronger coupling to the contacts, which allows the triad to move more electrons through it, absorbing more photons per unit time, and doing more work.

I. Introduction

In recent years, the efficient conversion of solar energy into chemical or electrical forms has attracted considerable attention.^{1–3} Among several proposals for light-harvesting devices,⁴ organic solar cells are advantageous for their low weight, high flexibility, and low manufacturing costs.^{5–7} In this work, we consider an artificial photosynthetic system where a donor–bridge–acceptor molecular triad serves as a basic light-converting element.^{8–11} To be specific, we consider a design (see Figure 1) where a molecule of porphyrin, P, acts as a photosensitive bridge inserted between the electron donor (e.g., a ferrocene molecule, Fc) and the electron acceptor (a fullerene molecule, C₆₀).^{12,13} We focused on this particular system because experiments have been made on it; so it works in the lab, but not that efficiently.

The molecule of ferrocene can be attached¹⁴ to a gold electrode (the left, L, lead in Figure 1), which injects electrons into the system. The acceptor molecule, C₆₀, is coupled to the electrolyte solution (the right, R, lead) containing molecules of oxygen, O₂, or methyl viologen, MV²⁺. These molecules are able to take electrons away from the fullerene and deliver them to the counter electrode on the right side of Figure 1. We note that C₆₀ molecules can also be directly connected to gold electrodes.¹⁵

It was shown¹⁴ that this ferrocene–porphyrin–fullerene triad generates a photocurrent with a quantum yield $\Phi \sim 25\%$. The clusters of coupled porphyrin–fullerene molecules can also be deposited on nanostructured semiconducting electrodes,⁷ with a resulting power-conversion (thermodynamic) efficiency $\eta \sim 2\%$. This number is lower than the efficiency of hybrid nanorod–polymer solar cells⁵ ($\eta \sim 6.9\%$) and is also lower than the efficiency of tandem polymer solar cells⁶ ($\eta \sim 6.5\%$).

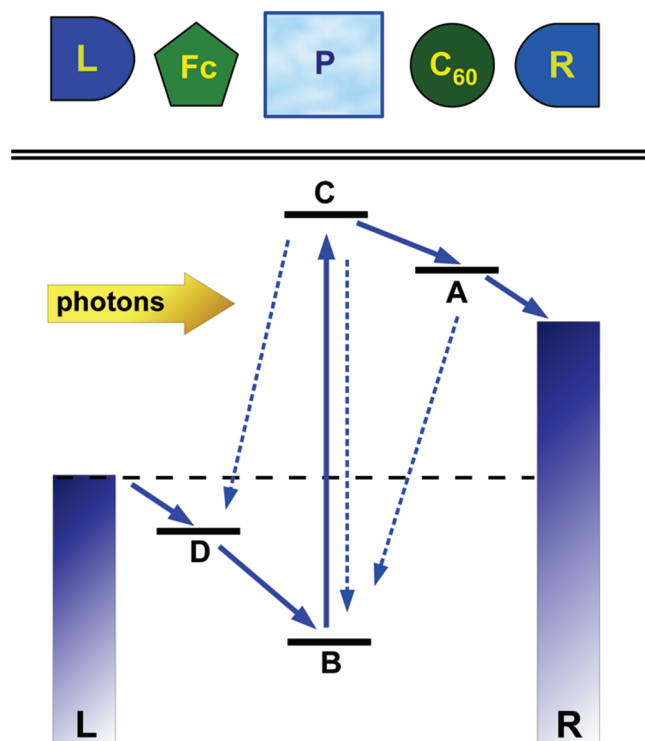


Figure 1. Schematic diagram of the molecular triad coupled to conducting leads and (below) its energy diagram. The ferrocene molecule, Fc, has a single energy level $E_D = -510$ meV. This molecule accepts electrons from the left lead, L, and serves as an electron donor, D, for the photosensitive porphyrin molecule P. The porphyrin molecule has two energy levels, $E_B = -1150$ meV and $E_C = 750$ meV. The transitions between these levels, B and C, are induced by the incident light. The fullerene molecule, C₆₀, is characterized by the single energy level $E_A = 620$ meV. The fullerene (the acceptor A) takes electrons from the upper level C of the porphyrin and transfers them to the right lead denoted as R. The electron transitions caused by radiation leakage are shown by dashed lines on the energy diagram.

* To whom correspondence should be addressed. E-mail: asmirnov@riken.jp; fnori@riken.jp.

[†] RIKEN.

[‡] University of Michigan.

[§] Queens College, CUNY.

Despite recent developments, organic solar cells based on porphyrin–fullerene complexes rank below other designs, both in efficiency and in generated power.^{1,4,5} Here, we analyze light-induced electron transport through a ferrocene–porphyrin–fullerene triad and show that for a reasonable set of parameters the power-conversion efficiency of such a cell can be more than 40% with a quantum yield exceeding 90%, which is much higher than the 25% quantum yield observed in experiments.¹⁴ We argue that such an increase in efficiency and in quantum yield can be achieved with a strong coupling of the triad to conducting leads.

II. Model and Parameters

Figure 1 shows the schematics and the energy diagram of the system under study. The donor (D) molecule (e.g., ferrocene), with an energy level E_D , is coupled to the left (L) electron reservoir. The acceptor (A) molecule (e.g., fullerene), with an energy level E_A , is coupled to the right (R) lead. The bridge molecule (e.g., porphyrin, P) has two energy levels, E_B and E_C , separated by a large energy gap. The bridge states, B and C, are tunnel-coupled both to the donor state D and the acceptor state A. Electron transitions between the lower bridge state B and the upper state C are induced by an external electromagnetic field (light) which is characterized by a frequency ω_0 and amplitude F . After such a transition, the electron from the upper bridge state C can be transferred to the acceptor A, whereas the lower bridge state B is populated by the donor D, thereby inducing an electron current through the structure.

Each electron state can be occupied by a single electron, since the electron spin can be neglected. Our analysis also considers the radiation-induced leakage from the excited levels C and A to the levels D and B. In addition to radiation leakage, the excited state C of the porphyrin molecule may relax to the ground state B due to quenching by the energy transfer to plasmonic modes of the gold electrode. To describe this quenching, we couple the levels B and C to an additional Ohmic heat bath. We do not consider here any specific details of the quenching process.

The high efficiency predicted in our calculations occurs due to our assumption of a stronger coupling to the leads, compared with previous experimental studies. Increasing the coupling strength leads to a more effective depopulation of the upper bridge level C and fast population of the lower bridge level B, to get them ready for the absorption of the next photon.

During the process of single-electron transfer,¹⁴ ferrocene can be either neutral, Fc, or positively charged, Fc^{*+} ; the porphyrin molecule changes from its uncharged form, P, to the positively charged form, P^{*+} ; and the fullerene switches between the neutral, C_{60} , and negatively charged form, C_{60}^- . Note that the anion porphyrin, P^{*-} , with one electron on level B and one electron on level C, has a negative charge.

The electron populations of the donor (D), bridge ($P = B$ and C), and acceptor (A) molecules are given by the operators $n_\sigma = a_\sigma^\dagger a_\sigma$, where $\sigma = D, B, C$, and A, and $a_\sigma^\dagger, a_\sigma$ are creation/annihilation Fermi operators describing an electron located on the level σ . In the absence of an additional electron, the ferrocene and porphyrin molecules are positively charged. Accordingly, the donor and bridge charges (in units of the electron charge modulus $|e|$) are given by $q_D = 1 - n_D$ and $q_P = 1 - n_B - n_C$, respectively. The charge of the acceptor is $q_A = -n_A$.

A. Energy Levels and Coulomb Interactions. For the energy levels, E_A, \dots, E_D , we choose the following values (in eV): $E_D = -0.51$, $E_B = -1.15$, $E_C = 0.75$, and $E_A = 0.62$.

These values correspond (with an opposite sign) to the redox potentials¹⁴ (measured with respect to Ag/AgCl) of the ferrocene (D), H₂P porphyrin (B and C), and fullerene (A) molecules.

For the electrostatic parameters u_{DP} , u_{DA} , and u_{PA} , describing donor–bridge, donor–acceptor, and bridge–acceptor Coulomb energies, respectively, we use the values (in meV): $u_{DP} = 200$, $u_{DA} = 95$, and $u_{PA} = 180$, related to the distances (in nm), $r_{DP} = 1.62$, $r_{DA} = 3.42$, and $r_{PA} = 1.8$, between the corresponding molecules at the dielectric constant, $\epsilon \sim 4.44$. The charging energy of the porphyrin is estimated as $u_P \sim 600$ meV.

B. Tunneling and Relaxation Rates. We assume that the donor–bridge (Δ_{DB} , Δ_{DC}) and acceptor–bridge (Δ_{AB} , Δ_{AC}) tunneling elements are close to the value, $\Delta_D \sim 7.9 \text{ cm}^{-1} \sim 1 \text{ meV}$, measured in ref 16 for the porphyrin–fullerene dyads. For the tunneling coefficient Γ_L , describing electron transitions between the left lead L and the donor D, we use the value $\Gamma_L \sim 1.2 \mu\text{eV}$ ($\sim 1800 \mu\text{s}^{-1}$), unless otherwise specified. According to eq 19, $\Gamma_L \sim 2\pi|T_{kl}|^2\rho(\epsilon_F)$, this value corresponds to the energy-independent ferrocene-gold electron tunneling factor, $|T_{kl}| \sim |T_L| = 6.5 \text{ cm}^{-1}$, measured in ref 17. Here, $\rho(\epsilon_F) \sim 0.3 \text{ eV}^{-1} \text{ atom}^{-1}$ is the electron density of states for the gold at the Fermi energy $\epsilon_F = 5.51 \text{ eV}$. We choose the lower rate of $0.12 \mu\text{eV}$ ($\sim 180 \mu\text{s}^{-1}$) for the tunneling rate Γ_R . This rate can be of the same order as the rate Γ_L , if the fullerene molecule is directly attached to the gold electrode, as in ref 15.

The dipole matrix elements of the triad, $d_{\sigma\sigma'}$, determine the interaction of the porphyrin molecule with the external electromagnetic field (d_{BC}), as well as the radiation leakage between the acceptor state A and the ground porphyrin state B (d_{AB}) and between the excited state C of the porphyrin and the donor state D (d_{DC}). Here, e is the electron charge. For the matrix elements $x_{\sigma\sigma'}$, we have the estimates (in nm) as $x_{BC} = 1$, $x_{AB} = x_{DC} = 0.75$, which correspond to the following radiation relaxation rates:

$$\tau_{C \rightarrow B}^{-1} \sim 2.6 \text{ ns}^{-1}, \quad \tau_{A \rightarrow B}^{-1} \sim 1.2 \text{ ns}^{-1}, \quad \text{and} \quad \tau_{C \rightarrow D}^{-1} \sim 0.4 \text{ ns}^{-1}$$

An additional heat bath, which simulates the quenching of the porphyrin excited state, P^* ($\equiv C$), by the gold electrode, can be roughly described by the Ohmic spectral function, $\chi_P''(\omega) = \alpha_P \omega$, with the dimensionless coupling constant α_P . This process has a time scale^{14,18} in the range from 24 ps up to 1 ns. We choose here a value $\alpha_P \sim 1.7 \times 10^{-6}$, which corresponds to the reasonable $C \rightarrow B$ quenching time $\tau_P \sim 0.1 \text{ ns}$.

It was shown in refs.^{14,18} that the energy quenching can be suppressed by introducing several molecular spacers between the triad and the gold electrode. The spacers increase the distance between the porphyrin molecule and the gold surface; thus, significantly decreasing the probability of the Förster energy transfer. However, with the introduction of spacers¹⁷ the lead-ferrocene electron tunneling coupling, given by the factor $|T_L|$, decreases as well, e.g., from $|T_L| = 6.5 \text{ cm}^{-1}$ to the much lower value $|T_L| = 0.06 \text{ cm}^{-1}$. Correspondingly, there should be an optimal distance between the photosensitive part of the triad and the electrode surface, resulting in the most efficient performance of the solar cell.

Under the so-called standard conditions, the intensity of light is assumed to be about the average solar insolation, $\sim 20 \text{ mW/cm}^2$, the temperature $T = 298 \text{ K}$, and the photon energy $\hbar\omega_0 = 2.0 \text{ eV}$.

C. Reorganization Energies. The effect of the environment on the electron transitions^{19,20} between the active sites σ and σ' is described by a set of reorganization energies $\lambda_{\sigma\sigma'}$. Here we find that the power-conversion efficiency η has the maximum, $\eta \sim 0.42$, in the range of the reorganization energies, $\lambda_{AB} =$

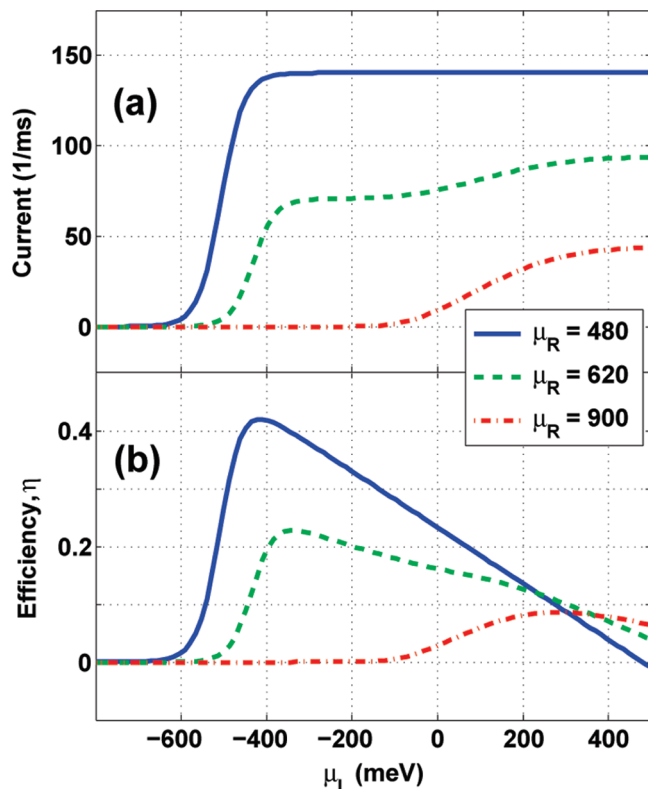


Figure 2. (a) Electron current and (b) the power-conversion efficiency η versus the chemical potential μ_L of the left lead for three values of the right-lead potential: $\mu_R = 480$ meV (blue continuous curve), $\mu_R = 620$ meV (green dashed curve), and $\mu_R = 900$ meV (red dashed-dotted curve).

$\lambda_{AC} = \lambda_A$, between 100 and 400 meV, when the parameter λ_D ($\lambda_D = \lambda_{DB} = \lambda_{DC}$) matches the energy difference between the D and B levels: $\lambda_D = 600$ meV $\approx (E_D - E_B)$. This value of λ_D is close to the reorganization energy obtained in ref 16. Hereafter, we assume that $\lambda_A = 400$ meV. It should be noted that the porphyrin-linked fullerenes are characterized by a very low reorganization energy,²¹ $\lambda \sim 230$ meV. The smallest value, $\lambda_{BC} = 100$ meV, is used for the light-induced intramolecular transition in the porphyrin moiety. To take into account a variation of the electron–phonon coupling during an electron transfer from the donor site D to the left lead L, and from the acceptor level A to the right electron reservoir R, we introduce the reorganization energy $\lambda_{LD} \sim 400$ meV. The fullerene molecule C_{60} has a more rigid structure than ferrocene (D), and, therefore, a smaller reorganization energy, $\lambda_{RA} \sim 200$ meV, can be expected for the $A \rightarrow R$ transition.

III. Results

We solve the set of master equations [see eq 11 in the Appendix of the paper] numerically and determine the probability $\langle \rho_{ii} \rangle$ to find the system in the energy eigenstate $|i\rangle$. This probability is substituted in the equation for the particle current and in the equations for the absorbed energy and the efficiency of the process.

A. Electron Current and Power-Conversion Efficiency versus Chemical Potential. In Figure 2 we show the dependence of the electron current and power-conversion efficiency η on the chemical potential of the left lead, μ_L , for various values of the chemical potential of the right lead, $\mu_R = 480, 620,$ and 900 meV. The potentials $\mu_R = 480$ and 620 meV correspond (with the opposite sign) to the redox energies of the oxygen,

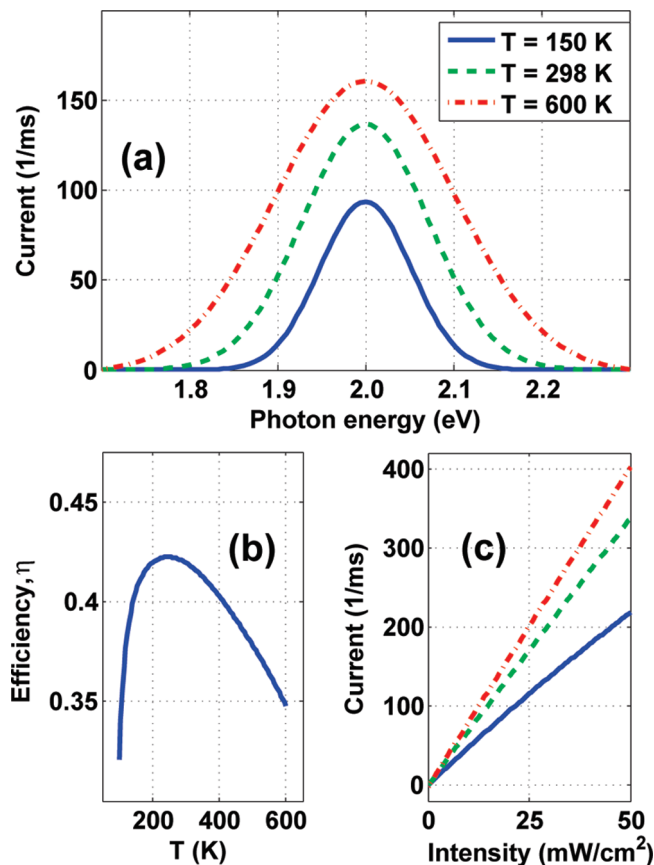


Figure 3. (a) Electron current as a function of the photon energy at different temperatures: $T = 150$ K (bottom blue continuous curve), $T = 298$ K (green dashed curve), and $T = 600$ K (top red dashed-dotted curve) and for the light intensity 20 mW/cm^2 . (b) Temperature dependence of the power-conversion efficiency η at the resonant photon energy, $\hbar\omega_0 = 2$ eV. Note that the power-conversion efficiency η has a maximum around room temperature. (c) Linear dependence of the current on the light intensity at $\hbar\omega_0 = 2$ eV and three temperatures, $T = 150, 298,$ and 600 K.

O_2 , and methyl viologen, MV^{2+} , molecules.¹⁴ These molecules can serve as electron carriers which accept electrons from the fullerene molecule C_{60} . We use the values of the parameters listed in the previous section.

The photoinduced current through the triad reaches its maximum, $I_R \sim 140$ electrons per ms, when $\mu_R = 480$ meV, and the potential μ_L exceeds the energy of the D -level, $\mu_L \geq -510$ meV, although the energetically uphill flow of electrons is observed at the lower value of μ_L as well. In the case when $\mu_L \geq -510$ meV, due to a relatively strong tunneling coupling between the level D and the left lead ($\Gamma_L \sim 1.8$ ns⁻¹), the electron transfer goes via the level D, which is quickly populated and depopulated. Then, a sufficiently strong current, I_R , combined with a high voltage, $V = \mu_R - \mu_L$, results in the maximum power-conversion efficiency, $\eta \approx 0.42$, at $\mu_L = -410$ meV and $\mu_R = 480$ meV. The current saturates as μ_L increases; however, the efficiency, which is proportional to the voltage V , decreases linearly. The distribution of electrons over the triad sites D, B, C, and A also depends on the electrochemical potential μ_R . Therefore, the turn-on potential μ_L for the current through the system is different for different values of μ_R .

B. Resonant Response of the Light-Induced Current versus Incident Photon Energy. The resonant behavior for the light-induced current as a function of the incident photon energy, $\hbar\omega_0$, is presented in Figure 3a for the electrochemical potentials $\mu_L = -410$ meV and $\mu_R = 480$ meV, light intensity ~ 20 mW/cm^2

cm², and for various temperatures (in K), $T = 150, 298,$ and 600 . The maximum number of electrons is pumped from the left to the right reservoir at the photon energy $\hbar\omega_0 = 2.0$ eV. Figure 3b, plotted at the resonance $\hbar\omega_0 = 2.0$ eV, shows that the power-conversion efficiency η is a nonmonotonic function of temperature with a high-performance plateau, $\eta \geq 0.4$, in the range from 150 to 400 K.

Figure 3c, which is also plotted at resonance and at the temperatures (in K): $T = 150, 298,$ and 600 , demonstrates that the photocurrent linearly increases with the light intensity. It should be noted that, at the fixed energy levels E_B and E_C , $E_B = -1.15$ eV, $E_C = 0.75$ eV, and the fixed frequency $\hbar\omega_0 = 2.0$ eV, the power-conversion efficiency η exceeds 40% in the range where 0.55 eV $< E_A < 0.85$ eV and -0.9 eV $< E_D < -0.5$ eV. This range includes the actual energy levels¹⁴ of the ferrocene molecule ($E_D = -0.51$ eV) and the fullerene ($E_A = 0.62$ eV).

C. Quantum Yield versus Coupling to the Leads. The tunnel coupling to the leads has a critical influence on the performance of the light-induced electron pump, drastically increasing its efficiency. To show this, in Figure 4a we plot the dependence of the quantum yield Φ (eq 29) on the L-to-D tunneling rate Γ_L . In Figure 4b, we show the quantum yield as a function of the rate Γ_R , describing the R-to-A electron tunneling. Both figures are plotted at the standard conditions for three values of the left-lead potential (in meV), $\mu_L = 0, -410, -520$, and at fixed $\mu_R = 480$ meV. We assume the rate $\Gamma_R = 180 \mu\text{s}^{-1}$ in Figure 4a and the rate $\Gamma_L = 1800 \mu\text{s}^{-1}$ in Figure 4b. The lower level of the left electron reservoir (more negative μ_L) corresponds to highly nonequilibrium conditions in the system. It is evident from Figure 4, panels a and b, that under weak nonequilibrium conditions ($\mu_L = 0, \mu_R = 480$ meV) the dependencies of the quantum yield Φ on both parameters, Γ_L [Figure 4a] and Γ_R [Figure 4b], are very similar. In this case the quantum yield reaches its saturation limit, $\Phi \geq 0.95$, starting from $\Gamma_L \geq 10 \mu\text{s}^{-1}$ [at $\Gamma_R = 180 \mu\text{s}^{-1}$, Figure 4a], and from $\Gamma_R \geq 20 \mu\text{s}^{-1}$ [at $\Gamma_L = 1800 \mu\text{s}^{-1}$, Figure 4b]. For these parameters, the power-conversion efficiency is low, $\eta \sim 0.23$. A much faster tunneling, $\Gamma_L \geq 1000 \mu\text{s}^{-1}$, between the left lead and the D-site is required under strong nonequilibrium conditions (at $\mu_L = -410$ meV) to keep the high quantum yield, $\Phi \geq 0.94$ [see Figure 4a]. In this case, electrons are pumped against the gradient $V = 0.89$ eV with a thermodynamic efficiency $\eta \geq 0.42$.

In the similar nonequilibrium state ($\mu_L = -410$ meV), the tunneling rate between the acceptor A and the right lead R can be much slower, $\Gamma_R \sim 200 \mu\text{s}^{-1}$, in order to maintain a high photon-to-electron quantum yield, $\Phi \sim 0.94$, and the power-conversion efficiency, $\eta \sim 0.42$ [see Figure 4b]. Note that the value of the gold-to-ferrocene tunneling coupling measured in ref 17 corresponds to the rate $\Gamma_L = 1800 \mu\text{s}^{-1}$. The rate of electron transfer, Γ_R , between the fullerene and the right lead is not known and was not controlled in experiments. It is evident from the green dashed curve in Figure 4b that the quantum yield, $\Phi = 25\%$, measured in ref 14, corresponds to the value $\Gamma_R \sim 0.2 \mu\text{s}^{-1}$ at $\mu_L = -410$ meV, $\mu_R = 480$ meV, and at $\Gamma_L = 1800 \mu\text{s}^{-1}$. It also corresponds to a power-conversion efficiency η of about 10%.

In recent experiments^{13,14,18} the alkanethiol–metal bonds are used to couple chromophores (porphyrins and fullerenes) to the electrode. The thiol–gold bonds are sufficiently strong, with a bonding energy²² of the order of 1.7 eV. The electrode–triad tunnelling can be increased by shortening the spacer length between the chromophore and the metal surface. However, the shorter spacer length results in the fast deactivation of the

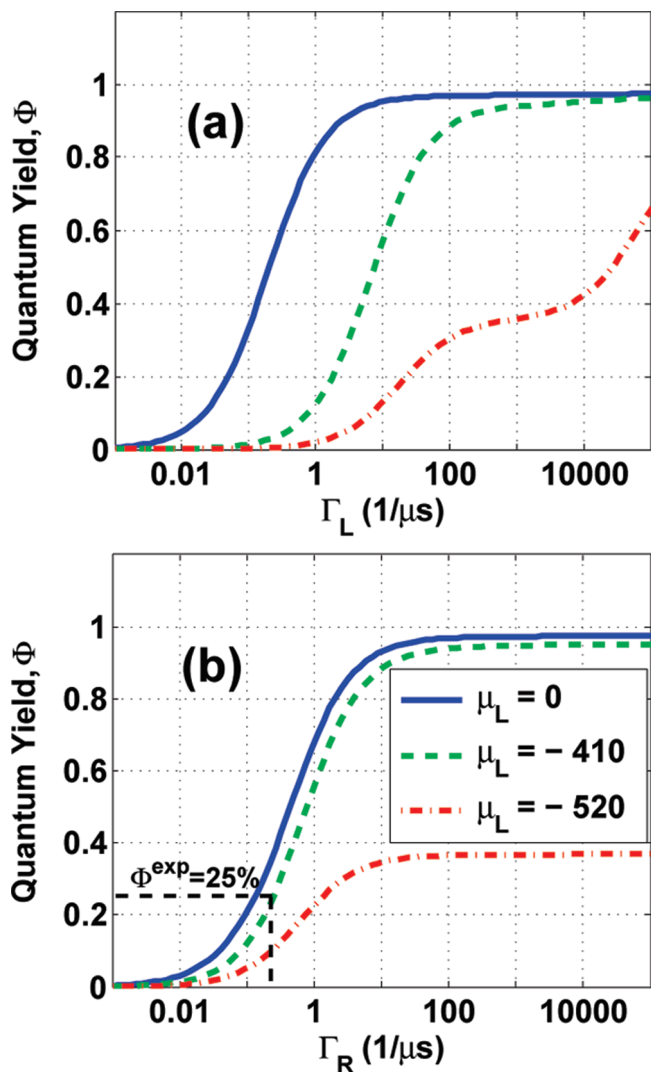


Figure 4. (a) Quantum yield Φ as a function of the tunnel coupling Γ_L between the left lead and the donor molecule at $\Gamma_R = 180 \mu\text{s}^{-1}$. (b) Quantum yield Φ as a function of the tunnel coupling Γ_R between the right lead and the acceptor molecule at $\Gamma_L = 1800 \mu\text{s}^{-1}$. The black dashed lines (horizontal and vertical) in (b) define the quantum yield, $\Phi^{\text{exp}} = 25\%$, achieved in experiments¹⁴ and the rate $\Gamma_R \approx 0.2 \mu\text{s}^{-1}$, corresponding to this quantum yield. Both graphs are plotted at $\mu_R = 480$ meV and at three values of the left electrochemical potential: $\mu_L = 0$ meV (top blue continuous curve), $\mu_L = -410$ meV (green dashed curve), and $\mu_L = -520$ meV (bottom red dashed-dotted curve).

chromophore excited state because of energy transfer to the electrode surface. This dissipative process is more pronounced for the gold leads than for the indium–tin–oxide (ITO) electrodes.¹⁸ It is expected that self-assembled monolayers of ferrocene–porphyrin–fullerene triads on the ITO surface could provide a basis for efficient and powerful light-to-electricity converting devices despite the lower electron transfer rate between the photoactive part and the ITO electrode.

IV. Conclusions

We have theoretically analyzed the performance of a photosensitive molecular triad coupled to two conducting leads. For a reasonable set of parameters, we have found the conditions when the photon-to-electron quantum yield exceeds 90% and the power-conversion efficiency of the device then becomes higher than 40%. What induces such a large predicted increase in the efficiency of this system? The stronger coupling to the

contacts, denoted here by Γ_L and Γ_R . Increasing the couplings to the contacts allows the system to move more electrons through it, absorbing more photons per unit time, and doing more work. In previous experiments,^{12–14} this coupling to the leads was not optimized and not well controlled. By controlling it and increasing the coupling to the leads, we predict a drastic increase in the energy-conversion efficiency.

Acknowledgment. This work was supported in part by the National Security Agency (NSA), Laboratory of Physical Science (LPS), Army Research Office (ARO), National Science Foundation (NSF) Grant No. EIA-0130383, and JSPS-RFBR 06-02-91200. L.M. was partially supported by the NSF NIRT under Grant No. ECS-0609146 and PSC–CUNY under Grant No. 60101-3940.

Appendix

In this Appendix we present a set of master equations, which describe electron transport through the molecular triad. We use methods of quantum transport theory^{23–29} complemented by elements of Marcus theory.^{19,20} More detailed derivations can be found in the Supporting Information.

A. Hamiltonian

We introduce the following creation/annihilation Fermi operators: $a_\sigma^\dagger, a_\sigma$ ($\sigma = D, B, C, \text{ and } A$). Correspondingly, the operators $n_\sigma = a_\sigma^\dagger a_\sigma$ describe the electron population of the σ -site. The basic Hamiltonian H_0 of the triad includes the energies E_σ of the sites and the Coulomb interactions between the sites, as

$$H_0 = \sum_{\sigma} E_{\sigma} n_{\sigma} + u_{\text{P}} n_{\text{B}} n_{\text{C}} + u_{\text{DP}} (1 - n_{\text{D}}) (1 - n_{\text{B}} - n_{\text{C}}) - u_{\text{DA}} (1 - n_{\text{D}}) n_{\text{A}} - u_{\text{PA}} (1 - n_{\text{B}} - n_{\text{C}}) n_{\text{A}} \quad (1)$$

where u_{P} is the charging energy of the porphyrin molecule, u_{DP} , u_{DA} , and u_{PA} are the electrostatic couplings of the donor and the bridge, the donor and the acceptor, and the bridge and the acceptor, respectively. The tunneling events between the electron sites are described by

$$H_{\text{tun}} = - \sum_{\sigma\sigma'} \Delta_{\sigma\sigma'} a_{\sigma}^{\dagger} a_{\sigma'} + \text{H.c.} \quad (2)$$

with matrix elements $\Delta_{\sigma\sigma'}$. Here, the indices σ, σ' sweep over all pairs, $\{D, B\}, \{D, C\}, \{A, B\}$, and $\{A, C\}$, coupled by direct tunneling, and the notation H.c. means a Hermitian conjugate.

Tunnel couplings of the donor to the left lead and the acceptor to the right lead are given by the Hamiltonian

$$H_{\text{tr}} = - \sum_k T_{\text{kL}} c_{\text{kL}}^{\dagger} a_{\text{D}} - \sum_k T_{\text{kR}} c_{\text{kR}}^{\dagger} a_{\text{A}} + \text{H.c.} \quad (3)$$

where $c_{\text{k}\alpha}^{\dagger}$ and $c_{\text{k}\alpha}$ are the creation/annihilation operators of an electron with a quasi-momentum k in the α lead ($\alpha = L, R$). The Hamiltonian of the leads is $H_{\text{LR}} = \sum_{\text{k}\alpha} \epsilon_{\text{k}\alpha} c_{\text{k}\alpha}^{\dagger} c_{\text{k}\alpha}$, whereas the Hamiltonian of the environment, composed of many harmonic oscillators,^{19,20} is given by

$$H_{\text{env}} = \sum_j \frac{p_j^2}{2m_j} + \sum_j \frac{m_j^2 \omega_j^2}{2} \left(x_j - \sum_{\sigma} x_{j\sigma} n_{\sigma} - \sum_{\alpha} x_{j\alpha} n_{\alpha} \right)^2 \quad (4)$$

with $n_{\alpha} = \sum_k c_{\text{k}\alpha}^{\dagger} c_{\text{k}\alpha}$. Here x_j, p_j, m_j , and ω_j are the coordinate, momentum, mass and frequency of the j oscillator of the environment, respectively. The parameters $x_{j\sigma}$ and $x_{j\alpha}$ determine

the strength of the interaction between the electron subsystem and the environment.

In the rotating-wave approximation (RWA), the light-induced transitions between the bridge sites B and C are described by

$$H_{\text{F}} = -F e^{i\omega_0 t} a_{\text{B}}^{\dagger} a_{\text{C}} + \text{H.c.} \quad (5)$$

where the field amplitude, $F = e \mathcal{E}_{\text{ext}} x_{\text{BC}}$, is proportional to the strength of the external electromagnetic field, \mathcal{E}_{ext} , projected on the direction of the dipole moment, $d_{\text{BC}} = e x_{\text{BC}}$, of the porphyrin molecule.

The absorption of a weak external electromagnetic field $f(t)$ (probe field) by the porphyrin molecule can be taken into account by introducing an additional term in the Hamiltonian: $H_{\text{probe}} = -f(t) \mathcal{P}$, where

$$\mathcal{P} = a_{\text{B}}^{\dagger} a_{\text{C}} + a_{\text{C}}^{\dagger} a_{\text{B}} \quad (6)$$

is the polarization operator. We note that for the field, $f(t) = F e^{i\omega_0 t} + \text{H.c.}$, the Hamiltonian H_{probe} has the same form as H_{F} provided that the RWA is valid.

To include the radiation leakage from the excited energy states C and A to the lower levels D and B, we add the coupling

$$H_{\text{rad}} = -Q_{\text{DC}} a_{\text{D}}^{\dagger} a_{\text{C}} - Q_{\text{AB}} a_{\text{A}}^{\dagger} a_{\text{B}} - Q_{\text{BC}} a_{\text{B}}^{\dagger} a_{\text{C}} + \text{H.c.} \quad (7)$$

to the radiation heat bath having the free Hamiltonian H_{Q} . The operators of the radiation bath, $Q_{\sigma\sigma'} = d_{\sigma\sigma'} \mathcal{C}_{\text{rad}}$, are proportional to the projection of the fluctuating electromagnetic field, \mathcal{C}_{rad} , along the direction of the corresponding dipole moment, $d_{\sigma\sigma'} = e x_{\sigma\sigma'}$.

The excited porphyrin molecule, P^* , can be quenched by the gold lead L. This loss of energy can be accounted for by adding a term, $H_{\text{quen}} = -Q_{\text{P}} \mathcal{P}$, to the total Hamiltonian H . Here, Q_{P} is the variable of this additional Ohmic bath with the Hamiltonian H_{P} , and \mathcal{P} is the porphyrin polarization operator, eq 6.

The total Hamiltonian H of the system includes all the above-mentioned terms, as

$$H = H_0 + H_{\text{F}} + H_{\text{tun}} + H_{\text{tr}} + H_{\text{probe}} + H_{\text{env}} + H_{\text{rad}} + H_{\text{quen}} + H_{\text{LR}} + H_{\text{Q}} + H_{\text{P}} \quad (8)$$

B. Basis States

The electron transport through the triad can be conveniently described^{26,27,29} in the basis of 16 occupational states: $|1\rangle = |\text{Vacuum}\rangle, |2\rangle = a_{\text{B}}^{\dagger} |1\rangle, |3\rangle = a_{\text{B}}^{\dagger} |2\rangle, \dots, |16\rangle = a_{\text{B}}^{\dagger} a_{\text{B}}^{\dagger} a_{\text{C}}^{\dagger} a_{\text{A}}^{\dagger} |1\rangle$. In this basis, H_0 is diagonal, $H_0 = \sum_{\mu} E_{\mu} |\mu\rangle \langle \mu|$, where $\mu = 1, \dots, 16$. The energy spectrum E_{μ} is determined by the Coulomb couplings and by the energies E_{σ} , involved in H_0 of eq 1. The electron operators of the triad ($a_{\sigma}, a_{\sigma}^{\dagger}, n_{\sigma}$) can be expressed in terms of the operators $\rho_{\mu\nu} = |\mu\rangle \langle \nu|$, for example, as

$$a_{\sigma} = \sum_{\mu\nu} a_{\sigma,\mu\nu} \rho_{\mu\nu}; \quad a_{\sigma}^{\dagger} a_{\sigma'} = \sum_{\mu\nu} (a_{\sigma}^{\dagger} a_{\sigma'})_{\mu\nu} \rho_{\mu\nu} \quad (9)$$

with the matrix elements

$$a_{\sigma,\mu\nu} = \langle \mu | a_{\sigma} | \nu \rangle; \quad (a_{\sigma}^{\dagger} a_{\sigma'})_{\mu\nu} = \langle \mu | a_{\sigma}^{\dagger} a_{\sigma'} | \nu \rangle \quad (10)$$

C. Master Equations

Using methods of quantum transport theory and the theory of open quantum systems,^{26,27} we derive (see the Supporting Information) a set of master equations for the probability, $\langle \rho_{\mu\mu} \rangle = \langle \rho_{\mu\mu} \rangle$, to find the system in the state μ , as

$$\langle \hat{\rho}_{\mu} \rangle = \sum_{\nu} (\kappa_{\mu\nu} + \gamma_{\mu\nu}) \langle \rho_{\nu} \rangle - \sum_{\nu} (\kappa_{\nu\mu} + \gamma_{\nu\mu}) \langle \rho_{\mu} \rangle \quad (11)$$

The relaxation matrix $\kappa_{\mu\nu}$ includes contributions from the direct tunneling between the sites σ and σ' , $\kappa_{\mu\nu}^{\text{tun}}$, from the optical transitions between the porphyrin levels B and C, $\kappa_{\mu\nu}^{\text{F}}$, and from the radiation leakage, $\kappa_{\mu\nu}^{\text{rad}}$. The first term is given by

$$\kappa_{\mu\nu}^{\text{tun}} = \sum_{\sigma\sigma'} \sqrt{\frac{\pi}{\lambda_{\sigma\sigma'} T}} |\Delta_{\sigma\sigma'}|^2 [|(a_{\sigma}^+ a_{\sigma'})_{\mu\nu}|^2 + |(a_{\sigma}^+ a_{\sigma'})_{\nu\mu}|^2] \exp\left[-\frac{(\omega_{\mu\nu} + \lambda_{\sigma\sigma'})^2}{4\lambda_{\sigma\sigma'} T}\right] \quad (12)$$

The reorganization energies^{19,20}

$$\lambda_{\sigma\sigma'} = \sum_j \frac{m_j \omega_j^2}{2} (x_{j\sigma} - x_{j\sigma'})^2 \quad (13)$$

correspond to the electron transfer between the sites σ and σ' .

The contribution of the photoinduced electron transitions between levels B and C to the relaxation matrix has the form

$$\kappa_{\mu\nu}^{\text{F}} = |F|^2 \sqrt{\frac{\pi}{\lambda_{\text{BC}} T}} |(a_{\text{B}}^+ a_{\text{C}})_{\mu\nu}|^2 \exp\left[-\frac{(\omega_{\mu\nu} + \omega_0 + \lambda_{\text{BC}})^2}{4\lambda_{\text{BC}} T}\right] + |F|^2 \sqrt{\frac{\pi}{\lambda_{\text{BC}} T}} |(a_{\text{B}}^+ a_{\text{C}})_{\nu\mu}|^2 \exp\left[-\frac{(\omega_{\mu\nu} - \omega_0 + \lambda_{\text{BC}})^2}{4\lambda_{\text{BC}} T}\right] \quad (14)$$

The contribution of the radiation leakage is given by

$$\kappa_{\mu\nu}^{\text{rad}} = \frac{2}{3} n_{\text{refr}} \sum_{\sigma\sigma'} |d_{\sigma\sigma'}|^2 [|(a_{\sigma}^+ a_{\sigma'})_{\mu\nu}|^2 + |(a_{\sigma}^+ a_{\sigma'})_{\nu\mu}|^2] \left(\frac{\omega_{\mu\nu}}{c}\right)^3 \left[\coth\left(\frac{\omega_{\mu\nu}}{2T}\right) - 1\right] \quad (15)$$

where n_{refr} is the refraction index of the medium, and the dipole moment, $d_{\sigma\sigma'}$, is assumed to be nonzero only for transitions between the levels $(\sigma, \sigma') = \{\text{AB}\}$, $\{\text{DC}\}$, and $\{\text{BC}\}$.

The loss of energy because of P^* quenching by a gold electrode is described by the rate $\kappa_{\mu\nu}^{\text{P}}$, which has a form similar to eq 15

$$\kappa_{\mu\nu}^{\text{P}} = \alpha_{\text{P}} |(a_{\text{B}}^+ a_{\text{C}})_{\mu\nu}|^2 + |(a_{\text{B}}^+ a_{\text{C}})_{\nu\mu}|^2 \omega_{\mu\nu} \left[\coth\left(\frac{\omega_{\mu\nu}}{2T}\right) - 1\right] \quad (16)$$

The total relaxation matrix, $\kappa_{\mu\nu}$, involved in eq 11, is equal to the sum of the above-mentioned contributions

$$\kappa_{\mu\nu} = \kappa_{\mu\nu}^{\text{tun}} + \kappa_{\mu\nu}^{\text{F}} + \kappa_{\mu\nu}^{\text{rad}} + \kappa_{\mu\nu}^{\text{P}} \quad (17)$$

The tunnel coupling of the triad to the L and R electron reservoirs leads to the following addition to the relaxation matrix: $\gamma_{\mu\nu} = \gamma_{\mu\nu}^{\text{L}} + \gamma_{\mu\nu}^{\text{R}}$, with the components

$$\gamma_{\mu\nu}^{\text{L}} = \Gamma_{\text{L}} |a_{\text{D}\mu\nu}|^2 [1 - \mathcal{F}_{\text{L}}(\omega_{\nu\mu} - \lambda_{\text{LD}})] + \Gamma_{\text{L}} |a_{\text{D}\nu\mu}|^2 \mathcal{F}_{\text{L}}(\omega_{\mu\nu} + \lambda_{\text{LD}}) \\ \gamma_{\mu\nu}^{\text{R}} = \Gamma_{\text{R}} |a_{\text{A}\mu\nu}|^2 [1 - \mathcal{F}_{\text{R}}(\omega_{\nu\mu} - \lambda_{\text{RA}})] + \Gamma_{\text{R}} |a_{\text{A}\nu\mu}|^2 \mathcal{F}_{\text{R}}(\omega_{\mu\nu} + \lambda_{\text{RA}}) \quad (18)$$

which are proportional to the energy-independent tunneling rates²³

$$\Gamma_{\alpha} = 2\pi \sum_k |T_{k\alpha}|^2 \delta(\omega - \varepsilon_{k\alpha}) \quad (19)$$

Here $\omega_{\mu\nu} = E_{\mu} - E_{\nu}$, and λ_{LD} and λ_{RA} are the reorganization energies [see eq 13] related to electron transitions between the

donor and the left lead, as well as between the acceptor and the right lead, respectively.

The electron reservoirs ($\alpha = L, R$) are characterized by the Fermi distributions $f_{\alpha}(\omega)$ with temperature T ($k_{\text{B}} = 1$, $\hbar = 1$) and electrochemical potentials μ_{L} and μ_{R} . Taking into account the effect of the electron–phonon interaction on the tunneling of electrons between the leads and the active sites results in the replacement¹⁷ of the standard Fermi distribution $f_{\alpha}(\Omega)$ by its modification $\mathcal{F}_{\alpha}(\Omega)$, as

$$\mathcal{F}_{\alpha}(\Omega) = \sqrt{\frac{\pi}{\lambda_{\alpha} T}} \int \frac{d\omega}{2\pi} f_{\alpha}(\omega) \exp\left[-\frac{(\omega - \Omega)^2}{4\lambda_{\alpha} T}\right] \quad (20)$$

where $\lambda_{\text{L}} = \lambda_{\text{LD}}$, $\lambda_{\text{R}} = \lambda_{\text{RA}}$, and $f_{\alpha}(\omega) = \{\exp[(\omega - \mu_{\alpha})/T] + 1\}^{-1}$.

D. Electron Current

The electron flow through the triad is described by the particle current^{23,24,26,27}

$$I_{\alpha} = \frac{d}{dt} \sum_k \langle c_{k\alpha}^{\dagger} c_{k\alpha} \rangle$$

In the approximation of weak coupling to the leads, this current is determined by the probability distribution $\langle \rho_{\mu} \rangle$, as

$$I_{\text{R}} = \Gamma_{\text{R}} \sum_{\mu\nu} |a_{\text{A}\mu\nu}|^2 \{ [1 - \mathcal{F}_{\text{R}}(\omega_{\nu\mu} - \lambda_{\text{RA}})] \langle \rho_{\nu} \rangle - \mathcal{F}_{\text{R}}(\omega_{\nu\mu} + \lambda_{\text{RA}}) \langle \rho_{\mu} \rangle \} \quad (21)$$

The usual electric current, I_{α}^{e} , is proportional to the particle current I_{α} , as $I_{\alpha}^{\text{e}} = eI_{\alpha}$. In the steady-state regime, when $\langle \dot{\rho}_{\mu} \rangle = 0$, we have $I_{\text{L}} = -I_{\text{R}}$.

E. Absorbed Energy

The average energy absorbed by the triad per second,³⁰ $\mathcal{C}_{\text{phot}}$, is defined by the expression

$$\mathcal{C}_{\text{phot}} = -\langle \dot{j}(t) \mathcal{P} \rangle \quad (22)$$

where $f(t) = F e^{i\omega_0 t} + F^* e^{-i\omega_0 t}$ is the external electromagnetic field, and

$$\mathcal{P} = e^{i\xi_{\text{BC}}} a_{\text{B}}^+ a_{\text{C}} + \text{H.c.} \quad (23)$$

is the polarization of the system. Here, $\xi_{\text{BC}} = \sum_j p_j (x_{j\text{B}} - x_{j\text{C}})$ is the stochastic phase generated by the environment and related to the electron transition between the states B and C. In linear approximation, when

$$\mathcal{P}(t) = \int dt_1 \varphi(t - t_1) f(t_1) \quad (24)$$

we introduce the response function of the system, $\varphi(\tau)$, and its Fourier transform, the susceptibility $\chi(\omega)$, as

$$\chi(\omega) = \int d\tau e^{i\omega\tau} \varphi(\tau) \quad (25)$$

Then, the average absorbed energy, $\mathcal{C}_{\text{phot}}$, is determined by the imaginary part, $\chi''(\omega_0)$, of the triad susceptibility taken at the frequency ω_0 of the external field, as

$$\mathcal{C}_{\text{phot}} = 2\omega_0 |F|^2 \chi''(\omega_0) \quad (26)$$

The dissipative environment (described in this case by the stochastic phase ξ_{BC} and the reorganization energy λ_{BC}) gives the main contribution to the loss of the optical energy. The

response function $\varphi(t, t_1)$ is proportional to the characteristic function of the Gaussian stochastic phase ξ_{BC} ,

$$\varphi(t, t_1) \sim \langle \exp\{i[\xi_{BC}(t) - \xi_{BC}(t_1)]\} \rangle \approx \exp[-\lambda_{BC}T(t - t_1)^2]$$

Consequently, for the amount of energy absorbed by the triad per second, we obtain

$$\begin{aligned} \mathcal{E}_{\text{phot}} = \omega_0 |F|^2 & \sqrt{\frac{\pi}{\lambda_{BC}T}} \sum_{\mu\nu} |(a_B^+ a_C)_{\mu\nu}|^2 \langle \rho_\mu - \rho_\nu \rangle \\ & \times \left(\exp\left[-\frac{(\omega_{\mu\nu} - \lambda_{BC} + \omega_0)^2}{4\lambda_{BC}T}\right] \right. \\ & \left. - \exp\left[-\frac{(\omega_{\mu\nu} - \lambda_{BC} - \omega_0)^2}{4\lambda_{BC}T}\right] \right) \end{aligned} \quad (27)$$

F. Power-Conversion Efficiency

The thermodynamic (or power-conversion) efficiency of the system, η , can be defined as the ratio

$$\eta = \frac{\mathcal{E}_{\text{pump}}}{\mathcal{E}_{\text{phot}}} \quad (28)$$

of the energy of electrons pumped from the L lead to the R lead per unit of time, $\mathcal{E}_{\text{pump}} = I_R V$, and the energy of photons absorbed per unit time, \mathcal{E}_{hot} . Here, $V = \mu_R - \mu_L$ is the voltage applied across the triad system. We include the modulus of electron charge, $|e|$, to the definition of the voltage difference and, therefore, measure the voltage in units of meV. The quantum yield, Φ , is determined by the ratio of the number of electrons pumped per second, $n_{\text{pump}} = I_R$, and the number of absorbed photons, $N_{\text{phot}} = \mathcal{E}_{\text{pump}}/\omega_0$, as

$$\Phi = \frac{n_{\text{pump}}}{N_{\text{phot}}} = \eta \times \frac{\omega_0}{V} \quad (29)$$

The efficiency η and the quantum yield Φ can also be expressed in percentages (by multiplying the original η and Φ by 100%).

Supporting Information Available: Detailed derivation of the system of master equations as well as formulas for an electron current and for absorbed energy. This material is available free of charge via the Internet at <http://pubs.acs.org>.

References and Notes

- (1) Crabtree, G. W.; Lewis, N. S. *Phys. Today* **2007**, *60* (3), 37–42.
- (2) LaVan, D. A.; Cha, J. N. *Proc. Natl. Acad. Sci. U.S.A.* **2006**, *103*, 5251–5255.
- (3) Hambourger, M.; Moore, G. F.; Kramer, D. M.; Gust, D.; Moore, A. L.; Moore, T. A. *Chem. Soc. Rev.* **2009**, *38*, 25–35.
- (4) Grätzel, M. *Nature* **2001**, *414*, 338–344.
- (5) Huynh, W. U.; Dittmer, J. J.; Alivisatos, A. P. *Science* **2002**, *295*, 2425–2427.
- (6) Kim, J. Y.; Lee, K.; Coates, N. E.; Moses, D.; Nguen, T.-Q.; Dante, M.; Heeger, A. J. *Science* **2007**, *317*, 222–225.
- (7) Imahori, H.; Umeyama, T. *J. Phys. Chem. C* **2009**, *113*, 9029–9039.
- (8) Gust, D.; Moore, T. A. *Science* **1989**, *244*, 35–41.
- (9) Kuciauskas, D.; Liddell, P. A.; Lin, S.; Stone, S. G.; Moore, A. L.; Moore, T. A.; Gust, D. *J. Phys. Chem. B* **2000**, *104*, 4307–4321.
- (10) Moore, T. A.; Moore, A. L.; Gust, D. *Philos. Trans. R. Soc. London B* **2002**, *357*, 1481–1498.
- (11) Wasielewski, M. R. *J. Org. Chem.* **2006**, *71*, 5051–5066.
- (12) Imahori, H. *Org. Biomol. Chem.* **2004**, *2*, 1425–1433.
- (13) Imahori, H. *Bull. Chem. Soc. Jpn.* **2007**, *80*, 621–636.
- (14) Imahori, H.; Yamada, H.; Nishimura, Y.; Yamazaki, I.; Sakata, Y. *J. Phys. Chem. B* **2000**, *104*, 2099–2108.
- (15) Park, H.; Park, J.; Lim, A. K. L.; Anderson, E. H.; Alivisatos, A. P.; McEuen, P. L. *Nature* **2000**, *407*, 57–60.
- (16) Imahori, H.; Yamada, H.; Guldi, D. M.; Endo, Y.; Shimomura, A.; Kundu, S.; Yamada, K.; Okada, T.; Sakata, Y.; Fukuzumi, S. *Angew. Chem., Int. Ed.* **2002**, *41*, 2344–2347.
- (17) Weber, K.; Hockett, L.; Creager, S. J. *Phys. Chem. B* **1997**, *101*, 8286–8291.
- (18) Yamada, H.; Imahori, H.; Nishimura, Y.; Yamazaki, I.; Kyu Ahn, T.; Kim, S. K.; Kim, D.; Fukuzumi, S. *J. Am. Chem. Soc.* **2003**, *125*, 9129–9139.
- (19) Marcus, R. A.; Sutin, N. *Biochim. Biophys. Acta* **1985**, *811*, 265–322.
- (20) Cherepanov, D. A.; Krishtalik, L. I.; Mulikidjanian, A. Y. *Biophys. J.* **2001**, *80*, 1033–1049.
- (21) Imahori, H.; Tkachenko, N. V.; Vehmanen, V.; Tamaki, K.; Lemmetyinen, H.; Sakata, Y.; Fukuzumi, S. *J. Phys. Chem. A* **2001**, *105*, 1750–1756.
- (22) Wang, W.; Lee, T.; Reed, M. A. *Rep. Prog. Phys.* **2005**, *68*, 523–544.
- (23) Meir, Y.; Wingreen, N. S.; Lee, P. A. *Phys. Rev. Lett.* **1993**, *70*, 2601–2604.
- (24) Weinmann, D.; Häusler, W.; Kramer, B. *Phys. Rev. Lett.* **1995**, *74*, 984–987.
- (25) Keiser, F. J.; Hänggi, P.; Kohler, S. *New J. Phys.* **2008**, *10*, 065013.
- (26) Smirnov, A. Yu.; Mourokh, L. G.; Nori, F. *Phys. Rev. E* **2008**, *77*, 011919.
- (27) Smirnov, A. Yu.; Mourokh, L. G.; Nori, F. *J. Chem. Phys.* **2009**, *130*, 235105.
- (28) Yeganeh, S.; Ratner, M. A.; Galperin, M.; Nitzan, A. *Nano Lett.* **2009**, *9*, 1770–1774.
- (29) Ghosh, P. K.; Smirnov, A. Yu.; Nori, F. *J. Chem. Phys.* **2009**, *131*, 035102.
- (30) Landau, L. D.; Lifshitz, E. M. *Statistical Physics, Part I*; Pergamon: Oxford, 1980.

JP906866G